COMPDYN 2011
ECCOMAS Thematic Conference on
Computational Methods in Structural Dynamics and Earthquake Engineering
M. Papadrakakis, M. Fragiadakis, V. Plevris (eds.)
Corfu, Greece, 25-28 May 2011

ANALYSIS OF THE VEHICLE-TRACK-STRUCTURE-SOIL DYNAMIC INTERACTION OF RAILWAY BRIDGES FOR HST

A. Romero, J. Domínguez, P. Galvín

Escuela Técnica Superior de Ingenieros. Universidad de Sevilla.
Camino de los Descubrimientos, 41092 Sevilla, Spain
aro@us.es, jose@us.es, pedrogalvin@us.es

Keywords: High speed train (HST), Soil structure interaction, Railway bridge, Resonant vibration.

Abstract. *The dynamic vehicle-track-bridge-soil interaction is studied on high speed lines. The analysis is carried out using a general and fully three dimensional multi-body-finite element-boundary element model, formulated in the time domain to predict vibrations due to the train passage over the bridge. The vehicle is modelled as a multi-body system, the track and the bridge are modelled using finite elements and the soil is considered as a homogeneous half-space by the boundary element method. Usually, moving force model and moving mass model are employed to study the dynamic response of bridges. In this work, the multi-body system allows one to consider the quasi-static and dynamic excitation mechanisms. Soil-structure interaction is taken into account on the dynamic behaviour on simply-supported short span bridges. The influence of soil-structure interaction is analysed in both resonant and non-resonant regimes.*

1 INTRODUCTION

Resonance phenomenon on railway bridges occurs when the loading frequency is close to a multiple of a natural frequency of the structure. In short-span bridges, actual operation velocity could be higher than resonance velocities. In that case, high level vibrations reached on resonance regime can result in problems to the security, passenger comfort and track stability. Therefore, the dynamic behaviour of railway bridges becomes an important design issue. Bridge behaviour is influenced by many factors such as the axle load, successive load passage and track irregularities. These effects are evaluated by dynamic amplification factors on railway bridge standards, which represent the amplification in the dynamic response in relation with the static response for a single moving load [1]. However, the dynamic amplification factors do not account for the resonance effects and its use is limited to trains speed below 220 km/h. In other cases, it is required further analysis.

References about the dynamic response of railway bridges are quite extensive. Frýba [2] presented a theoretical model of a bridge using the integral transformation method. An estimation of the amplitude of the free vibration was given. Li et al. [3] investigated the influence of the vehicle-bridge interaction on resonant vibrations. They concluded that the maximum response in resonant regime is reached at the first resonance velocity. Ju et al. [4] suggested a three-dimensional finite element model to study resonant effects on multi-span bridges, concluding that loading frequencies and natural frequencies of bridges should be as different as possible to avoid resonance phenomenons. Xia et al. [5] investigated the resonance mechanisms and conditions of train-bridge system, analysing the resonant regimens according to their excitation mechanisms.

One of the first steps in the study of railway bridge vibrations is to develop an accurate model of the induced force by the train. Different vehicle-bridge interaction models have been used: moving load model, moving mass model and moving oscillators models. The moving force model is the simplest vehicle-bridge interaction model. The model can be used if the train speed is low enough to neglect its inertia. The model has been widely employed by the scientific comunity [6, 7, 8, 9]. Most sophisticated model is the moving mass model. This model takes into account the mass of the vehicle, but the model does not consider the effect of the suspension. Finally, comprehensive moving oscillator models have been used by several authors [3, 4, 5, 10, 11]. Pesterev et al. [10] examined the asymptotic behaviour of the moving oscillator for large and small values of the suspension. For infinite spring stiffness, the moving oscillator model is not equivalent to the moving mass model. Liu et al. [11] studied under which conditions dynamic train-bridge interaction must be considered for the dynamic analysis of railway bridges. They have concluded that the dynamic vehicle-bridge interaction is more important for large train-bridge mass ratio. Li and Su [3] established that the dynamic vehicle-bridge interaction leads a lower level dynamic response of the bridge than the moving force model.

The number of publications about the influence of soil-structure interaction (SSI) on railway bridges vibrations is reduced. Takemiya et al. [12, 13] studied the soil-foundation-bridge interaction under moving loads using a dynamic substructure method in the frequency domain. Recently, Ülker-Kaustell et. al [14] presented a qualitative analysis of dynamic the soil-structure interaction on a frame railway-bridge. That work is based on Takemiya's work.

In this work, a three dimensional numerical model is developed to study vehicle-track-structure-soil interaction (Fig. 1). The numerical model is based on the three dimensional finite element and boundary element formulation in the time domain. The articulated train con-

figuration is modelled as a multi-body system. Therefore, quasi-static and dynamic excitation mechanisms are considered.

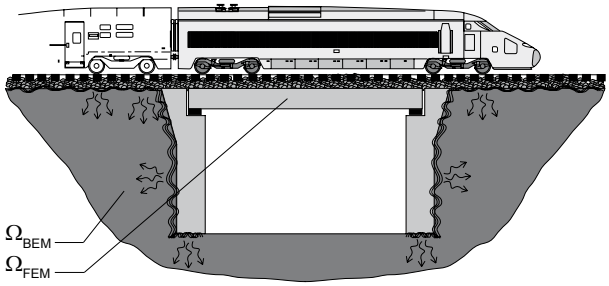

Figure 1: Vehicle-track-structure-soil interaction.

The outline of this papers is as follows. First, the numerical model is presented, including a brief summary of finite element and boundary element time domain formulation, and the multi-body model used to represent the vehicle-track-structure-soil interaction. Second, the influence of soil-structure interaction on the dynamic properties of the bridge is analysed. Third, the contribution of the dynamic excitation mechanisms due to high speed train passage are studied. Finally, induced vibrations on a simply-supported short span bridge are computed for several train speeds. Resonant and non-resonant regimes are studied. The influence of soil-structure interaction in the vibrations of railway bridge is considered.

2 Soil-structure interaction model

The model is based on the three-dimensional finite element [15] and boundary element [16] time domain formulations.

The boundary element method system of equations can be solved step-by-step to obtain the time variation of the boundary unknowns; i.e. displacements and tractions. Piecewise constant time interpolation functions are used for tractions and piecewise linear functions for displacements. Nine node rectangular quadratic elements are used for spatial discretization. Explicit expressions of the fundamental solution of displacements and tractions corresponding to an impulse point load in a three dimensional elastic full-space can be seen in reference [17].

Once the spatial and temporal discretizations are carried out it is obtained the following equation for each time step:

$$\begin{aligned} &\mathbf{H}^{nn}\mathbf{u}^n = \mathbf{G}^{nn}\mathbf{p}^n + \\ &\sum_{m=1}^{n-1}(\mathbf{G}^{nm}\mathbf{p}^m - \mathbf{H}^{nm}\mathbf{u}^m)\exp\left[-2\pi\alpha(n-m)\Delta t\right] \end{aligned} \tag{1}$$

where, $\mathbf{u}^n$ is the displacement vector and $\mathbf{p}^n$ is the traction vector at the end of the time interval n, and $\mathbf{H}^{nn}$ and $\mathbf{G}^{nn}$ are the full unsymmetrical boundary element system matrices, in the time interval n, α is the soil attenuation coefficient and Δt is the time step. An approach based on the classical Barkan expression [18] is employed to account for the material damping in the soil; the right hand side term derived from previous steps is damped by an exponential coefficient α using a linearly increasing exponent with time.

The equation which results from the finite element method can be expressed symbolically as follows if an implicit time integration Newmark method is applied [19]:

$$\mathbf{D}^{nn}\mathbf{u}^n = \mathbf{f}^n + \mathbf{f}^{n-1} \tag{2}$$

where $\mathbf{D}^{nn}$ is the dynamic stiffness matrix, $\mathbf{u}^n$ the displacement vector and $\mathbf{f}^n$ the equivalent force vector, in the time interval n.

In this paper, damping matrix **C** is considered proportional to mass matrix **M** and stiffness matrix **K**:

$$\mathbf{C} = \alpha_0 \mathbf{M} + \alpha_1 \mathbf{K} \tag{3}$$

α_0 and α_1 are obtained from i^{th} and j^{th} modal damping ratios (ζ_i and ζ_j, respectively). The n^{th} modal damping ratio is [20]:

$$\zeta_n = \frac{\alpha_0}{2\omega_n} + \frac{\alpha_1 \omega_n}{2} \tag{4}$$

The i^{th} and j^{th} modes should be chosen to obtain the damping ratios for all modes that contribute at the response. If both modes have the same damping ratio ζ, it is obtained:

$$\alpha_0 = \zeta \frac{2\omega_i \omega_j}{\omega_i + \omega_j} \quad \alpha_1 = \zeta \frac{2}{\omega_i + \omega_j} \tag{5}$$

Coupling boundary element and finite element sub-regions entails satisfying equilibrium and compatibility conditions at the interface between both regions [21].

3 Vehicle model

The multi-body model used to represent the vehicle-structure-soil dynamic interaction is shown in figure 2.(a). Axles and car bodies are considered rigid parts. Primary and secondary suspensions are represented by spring and damper elements [22].

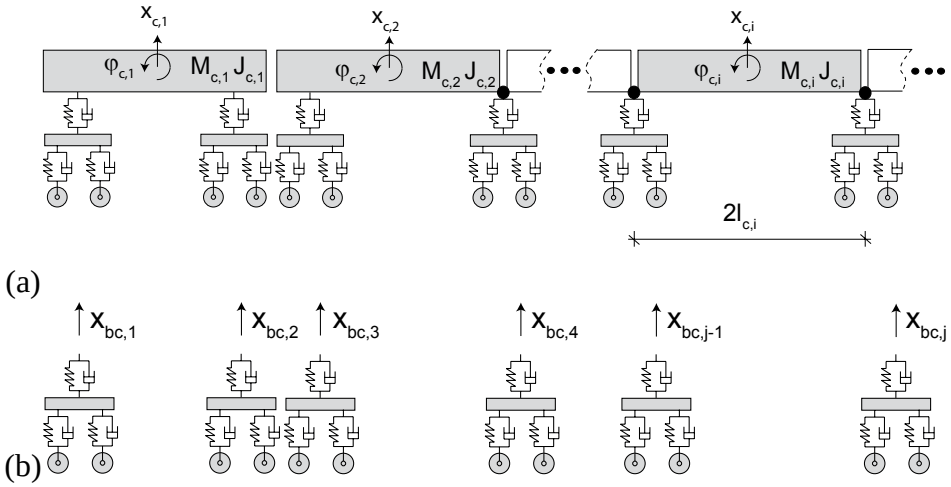

Figure 2: (a) The multi-body model for an articulated HST. (b) Uncoupled bogies.

The equations of motion for the uncoupled multi-body system shown in Fig. 2.(b) can be written as follows:

$$\tilde{\mathbf{M}}\ddot{\mathbf{x}} + \tilde{\mathbf{C}}\dot{\mathbf{x}} + \tilde{\mathbf{K}}\mathbf{x} = \tilde{\mathbf{F}} \tag{6}$$

where, $\tilde{\mathbf{M}}$, $\tilde{\mathbf{C}}$ and $\tilde{\mathbf{K}}$ are the mass, damping and stiffness matrices, respectively. Vehicle response is described by the displacement x_c and rotation φ_c of the body, the displacement x_b and rotation φ_b of the bogies, and the displacement of the wheels x_{wr} and x_{wf}.

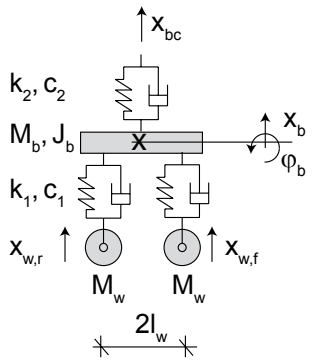

Figure 3: The multi-body model for a bogie.

The mass matrix of each bogie (Eq. 7) is composed of the bogie mass M_b, the bogie inertia moment J_b and wheel masses M_w:

$$\mathbf{M}_b = diag\,(0\ M_b\ J_b\ M_w\ M_w) \tag{7}$$

The stiffness and damping matrices of a bogie can be written as:

$$\mathbf{K}_b = \begin{pmatrix} k_2 & -k_2 & 0 & 0 & 0 \\ -k_2 & 2k_1+k_2 & 0 & -k_1 & -k_1 \\ 0 & 0 & 2k_1 l_w^2 & -k_1 l_w & k_1 l_w \\ 0 & -k_1 & -k_1 l_w & k_1 & 0 \\ 0 & -k_1 & k_1 l_w & 0 & k_1 \end{pmatrix} \tag{8}$$

$$\mathbf{C}_b = \begin{pmatrix} c_2 & -c_2 & 0 & 0 & 0 \\ -c_2 & 2c_1+c_2 & 0 & -c_1 & -c_1 \\ 0 & 0 & 2c_1 l_w^2 & -c_1 l_w & c_1 l_w \\ 0 & -c_1 & -c_1 l_w & c_1 & 0 \\ 0 & -c_1 & c_1 l_w & 0 & c_1 \end{pmatrix} \tag{9}$$

where, k_1 and c_1 are the stiffness and damping of the primary suspension, k_2 and c_2 are the stiffness and damping of the secondary suspension, and $2l_w$ is the distance between axles of a bogie.

The equation of motion of the whole train can be obtained from displacement relationships between car bodies and bogies. The relationshisp to obtain the equation of motion of the front traction car [22] are:

$$\begin{aligned} x_{bc,1} &= x_{c,1} - \varphi_{c,1} l_c \\ x_{bc,2} &= x_{c,1} + \varphi_{c,1} l_c \end{aligned} \tag{10}$$

where, $x_{c,1}$ and $\varphi_{c,1}$ represent vertical displacement and rotation of the car body, respectively, and $2l_c$ the bogie distance in a vehicle. Similar expression can be drawn for the first passenger car (Fig. 2). The vertical displacement $x_{bc,n}$ for the m^{th} vehicle can be written as follows:

$$x_{bc,n} = 2\sum_{i=3}^{m}\left((-1)^{n+i} x_{c,i}\right) + (-1)^n \left(x_{c,2} + l_{c,2}\varphi_{c,2}\right) \tag{11}$$

The relationships for the whole train can be expressed as:

$$\mathbf{x}_{bc} = \mathbf{L}\mathbf{x}_c \tag{12}$$

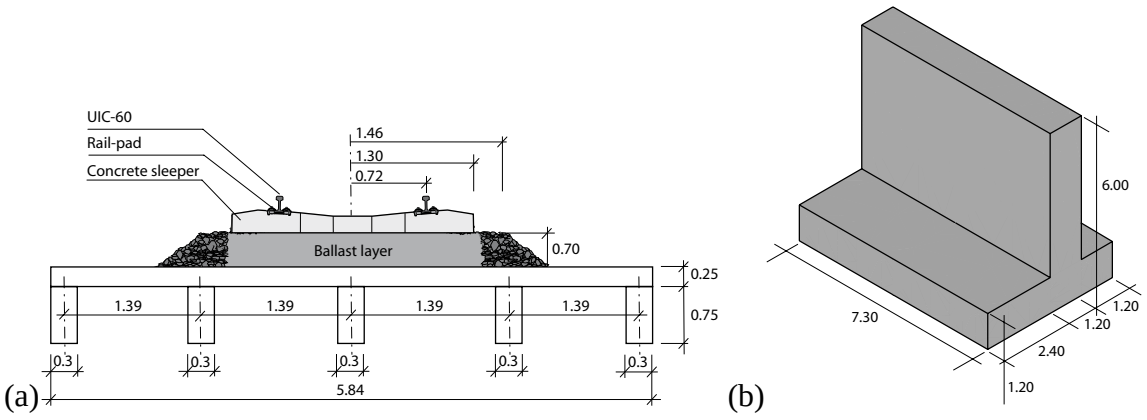

Figure 4: (a) Deck cross-section. (b) Abutment geometry.

Introducing Eq. (12) into Eq. (6) lead to:

$$\mathbf{M}\ddot{\mathbf{x}} + \mathbf{C}\dot{\mathbf{x}} + \mathbf{K}\mathbf{x} = \mathbf{F} \tag{13}$$

where, **M**, **C** and **K** are the mass, damping and stiffness matrices of the articulated HST (Fig. 2.(a)). The mass matrix is obtained by assembling car body mass matrix:

$$\mathbf{M}_c = diag\,(M_c\ J_c) \tag{14}$$

where M_c is the mass of the car body and J_c the inertia moment of the car body. The degree of freedom of rotation of the vehicle allows us to consider the pitch car inertia moment.

Finally, the equation of motion of the vehicle is introduced in the soil-structure interaction equation imposing equilibrium and compatibility conditions at each wheel-rail contact point. A Hertzian contact spring is considered between wheels and rails [22, 23]. As vehicle moves along the track according to its speed, contact points between wheels and rails change as time goes on. A moving node is created at each wheel-rail contact point in the rail to couple vehicles and track. So the track mesh including rail changes at each time step. Then, mass, damping and stiffness matrices vary at each time step and the obtained finite element system of equations becomes non-linear. Nevertheless, the time domain formulation allows one to solve the non-linear system of equations using, for example, the methodology presented in reference [24].

4 Dynamic behaviour of simply-supported short span bridge

In this section, the dynamic behaviour of a simply-supported short span bridge under HST passage is studied. First, the modal properties are obtained account for soil-structure interaction. Second, the quasi-static and the dynamic load contribution are studied. Finally, the dynamic response of the bridge due to HST passage is analysed taken into account soil-structure interaction.

4.1 Soil-structure dynamic interaction

In this paper a railway bridge with a single suported slab bay of $12\,\mathrm{m}$ is studied. The deck (Fig. 4.(a)) is composed of a $0.25\,\mathrm{m}$ thickness concrete slab. The slab resting over five pre-stressed concrete beams with a $0.75 \times 0.3\,\mathrm{m}$ rectangular cross-section. A distance $1.39\,\mathrm{m}$ between beams is considered. The concrete has a density $\rho = 2500\,\mathrm{kg/m^3}$, a Poisson ratio $\nu = 0.2$, and a Young's modulus $E = 31 \times 10^9\,\mathrm{N/m^2}$.

The deck leans over two concrete abutments (Fig. 4.(b)) with density $\rho = 2500\,\text{kg/m}^3$, a Poisson ratio $\nu = 0.3$, and a Young's modulus $E = 20 \times 10^9\,\text{N/m}^2$. Beams resting on laminated rubber bearings. The bearings have a thickness of $20\,\text{mm}$ and the stiffness and damping values are $k_b = 560 \times 10^6\,\text{N/m}$ and $c_{rp} = 50.4 \times 10^3\,\text{Ns/m}$.

A single ballast track is located over the deck. The track is composed of two UIC60 rails with a bending stiffness $EI = 6.45 \times 10^6\,\text{Nm}^2$ and a mass per unit length $m = 60.3\,\text{kg/m}$ for each rail. The rail-pads have a $10\,\text{mm}$ thickness and their stiffness and damping values are $k_{rp} = 150 \times 10^6\,\text{N/m}$ and $c_{rp} = 13.5 \times 10^3\,\text{Ns/m}$, respectively. The prestressed concrete monoblock sleepers have a length $l = 2.50\,\text{m}$, a width $w = 0.235\,\text{m}$, a height $h = 0.205\,\text{m}$ (under the rail) and a mass $m = 300\,\text{kg}$. A distance $d = 0.6\,\text{m}$ between the sleepers is considered. The ballast has a density $\rho = 1800\,\text{kg/m}^3$, a Poisson ratio $\nu = 0.2$, and a Young's modulus equal to $E = 209 \times 10^6\,\text{N/m}^2$. The width of the ballast equals $2.92\,\text{m}$ and the height $h = 0.7\,\text{m}$.

The structure is assumed to be located at the surface of a homogeneous half-space that represents a stiff soil, with a S-wave velocity $C_s = 400.0\,\text{m/s}$, a P-wave velocity $C_p = 799.4\,\text{m/s}$, and a Rayleigh wave velocity $C_R = 372.6\,\text{m/s}$.

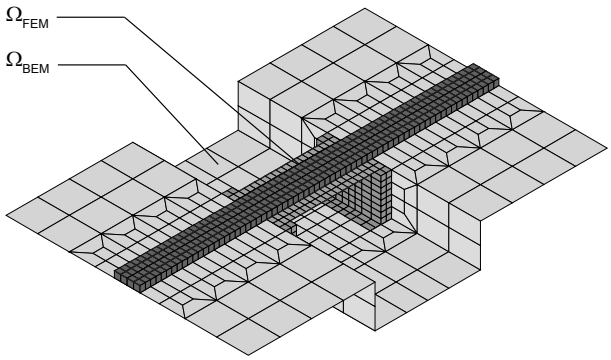

Figure 5: Soil-structure discretization.

Fig. 6 shows the first four mode shapes, corresponding with the first bending (symmetric), the first torsional, the first bending of cross-section (symmetric) and the first antisymmetric bending deck mode shapes, respectively.

Fig. 7 shows the vertical displacement at the center of the mid-span deck due to an impulsive load $P(t) = -1\,\text{N}\,(H(t) - H(t - 0.045\,\text{s}))$ acting in both rails. The response is governed by the first bending (symmetric) deck mode. The same structural damping is considered for all modes that contribute significantly to the response of the structure $\zeta = 2\,\%$. Damping matrix (Eq. 2) is obtained considering $\omega_i = \omega_1$ and $\omega_j = \omega_4$, being $\alpha_0 = 2.3$ and $\alpha_1 = 1.24 \times 10^{-4}$. Fig. 7 shows that the resonant frequency moves to $\tilde{f}_1 = 11.06\,\text{Hz}$ and an amplification in the response when SSI is considered. This effect is due to the additional level of flexibility between the abutments and the soil. The damping can be obtained from the free vibration response. Its value increases to $\tilde{\zeta} = 3.9\,\%$ when SSI is considered.

4.2 Quasi-static and dynamic excitation mechanisms

Induced vibrations due to HST passage are generated by several excitation mechanisms: the quasi-static contribution, the parametric excitation due to the discrete support of the rails and the dynamic contribution due to wheel and rail unevenness. In this section, the different excitation mechanisms are studied.

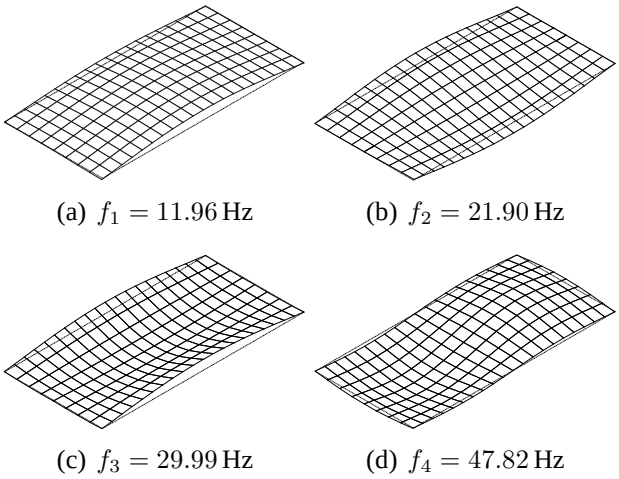

(a) $f_1 = 11.96\,\text{Hz}$ (b) $f_2 = 21.90\,\text{Hz}$

(c) $f_3 = 29.99\,\text{Hz}$ (d) $f_4 = 47.82\,\text{Hz}$

Figure 6: First four modes of vibrations of the structure.

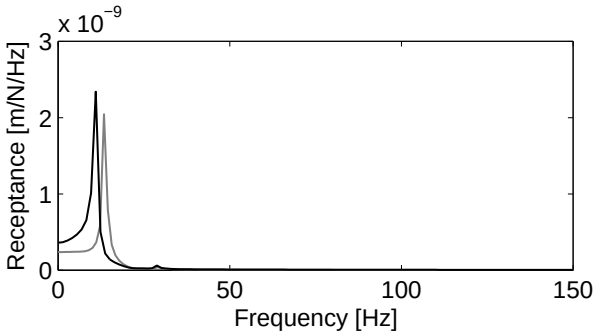

Figure 7: Track-structure-soil and track-structure receptance

Usually, the quasi-static contribution is modelled as moving constant forces and inertia effects of the vehicle are neglected. In this paper, the proposed multi-body system allows one to consider the sprung masses and the vehicle's suspension. Fig. 8 shows the articulated HST studied in this work. The train system consists of one front traction car, eight passenger cars and one rear traction car. Passenger cars adjacent to traction cars share one bogie with the neighbouring passenger car, while central passenger cars share both bogies with the neighbouring cars. Bogie distances, l_b, and axle distances, l_a, are shown in Fig. 8. The mechanical properties of the HST are summarized in table 1.

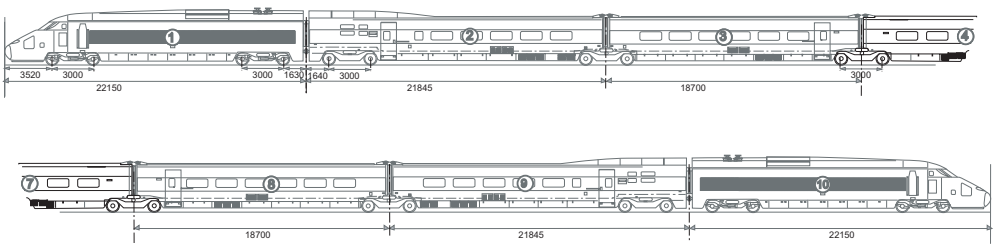

Figure 8: HST configuration.

Description	Name	Unit	Traction cars	Passenger cars
Mass of car-body	M_c	kg	55790	24000
Mass of bogie	M_b	kg	2380	3040
Mass of wheel-axle	M_w	kg	2048	2003
Car-body inertia moment	J_c	$kg\,m^2$	1.15×10^3	1.48×10^3
Bogie inertia moment	J_b	$kg\,m^2$	1.48×10^6	2.68×10^3
Primary suspension stiffness	k_1	N/m	2.45×10^6	1.4×10^6
Secondary suspension stiffnessa	k_2	N/m	2.45×10^6	0.82×10^6
Primary suspension damping	c_1	Ns/m	20×10^3	10×10^3
Secondary suspension damping	c_2	Ns/m	40×10^3	48×10^3

Table 1: Mechanical properties of HST

The transmitted load by an axle can be computed as the elastic interaction force F_H at wheel-rail contact point as follows:

$$F_H = -2k_H(u_c - u_w) \tag{15}$$

where, u_c is the rail displacement at contact point, u_w represents the wheel displacement and $k_H = 1.4 \times 10^9$ N/m is a Hertzian contact spring between wheels and rail [23]. Fig. 9 shows the one-third octave band spectra of the transmitted load for train speed $v = 80$ m/s and $V_{1,2} = 110.14$ m/s. $V_{1,2}$ is resonant resonant speed of the bridge (see section 4.3). The computed results are compared with those obtained using a moving force model. Both models lead to the same results at the bogie passing frequency, $f_b = v/l_b$, and the axle passing frequency, $f_a = v/l_a$. However, the computed transmitted forces present differences at higher frequencies due to inertia effects are neglected in the moving force model.

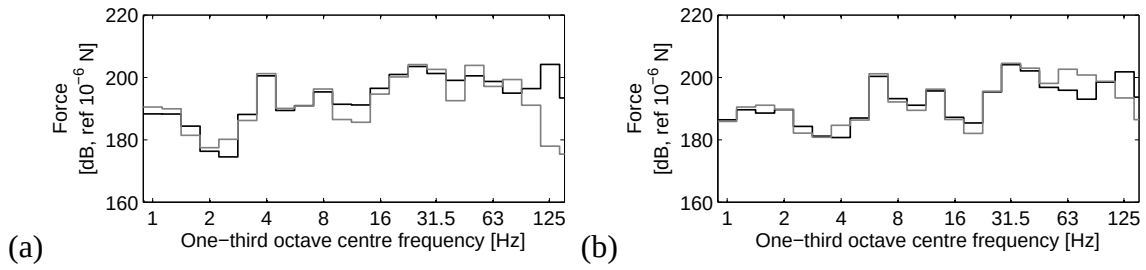

Figure 9: Excitation force on the track computed with a moving force model (grey line) and the multi-body system (black line) for a HST travelling at (a) $v = 80$ m/s and (b) $V_{1,2} = 110.14$ m/s

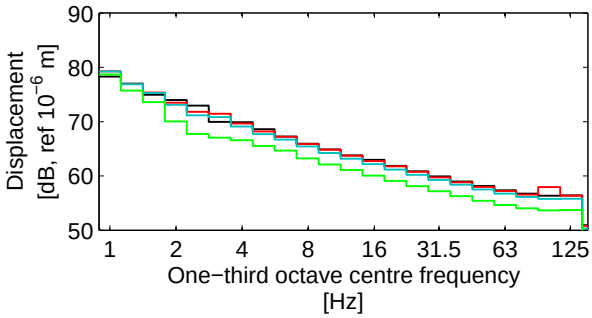

Figure 10: One-third octave band spectra of the vertical displacement at the wheel (red line), bogie (blue line) and the car body (green line) due to the track unevenness (black line) for a HST travelling at $v = 80\,\text{m/s}$.

The dynamic contribution account for track and wheel irregularities. The displacement vector u_c is equal to the sum of rail displacement u_r and rail unevenness $u_{w/r}$ perceived by an axle [25, 26]:

$$u_c = u_r + u_{w/r} \tag{16}$$

In this paper, random track unevenness $u_{w/r}(x)$ is modelled as a stationary Gaussian random process characterized by its one-sided PSD function $\tilde{S}_{u_{w/r}}(k_y)$. The spectral representation theorem is used to generate samples of track unevenness $u_{w/r}(x)$ as a superposition of harmonic functions with random phase angles [25, 26]:

$$u_{w/r}(x) = \sum_{m=1}^{n} \sqrt{2\tilde{S}_{u_{w/r}}(k_{ym})\Delta k_y}\cos(k_{ym}y - \theta_m) \tag{17}$$

where $k_{ym} = m\Delta k_y$ is the wavenumber sampling used only to compute the artificial profile, Δk_y the wavenumber step and θ_m are independent random phase angles uniformly distributed in the interval $[0, 2\pi]$. The artificial track profile is generated from PSD function according to ISO 8608 [27]:

$$\tilde{S}_{u_{w/r}}(k_y) = \tilde{S}_{u_{w/r}}(k_{y0})\left(\frac{k_y}{k_{y0}}\right)^{-w} \tag{18}$$

An artificial profile is obtained from the PSD function with $k_{y0} = 1\,\text{rad/m}$ and $\tilde{S}_{u_{w/r}}(k_{y0}) = 2\pi \times 10^{-8}\,m^3$. $w = 3.5$ is commonly assumed for wheel-rail unevenness in current high speed lines.

Fig. 10 shows the one-third octave band spectra of the vertical displacement at the wheel, bogie and body car due to the unevenness profile shown in the same figure. Primary and secondary suspensions system isolate body car and bogie at frequencies higher than $1.2\,\text{Hz}$ y $5.5\,\text{Hz}$, respectively.

Figs. 11(a),(b) show the one-third octave band spectra of the vertical acceleration at the center of the mid-span deck for a train passage at $v = 80\,\text{m/s}$ and $V_{1,2} = 110.14\,\text{m/s}$, respectively. The quasi-static contribution are represented in these figures. The deck response is governed by the quasi-static contribution.

4.3 Induced vibrations due to HST

In this section, SSI effect on induced vibrations due to HST passage is studied. Resonant and non resonant regimes are analysed. The geometry and the mechanical properties of the bridge have been described in previous sections.

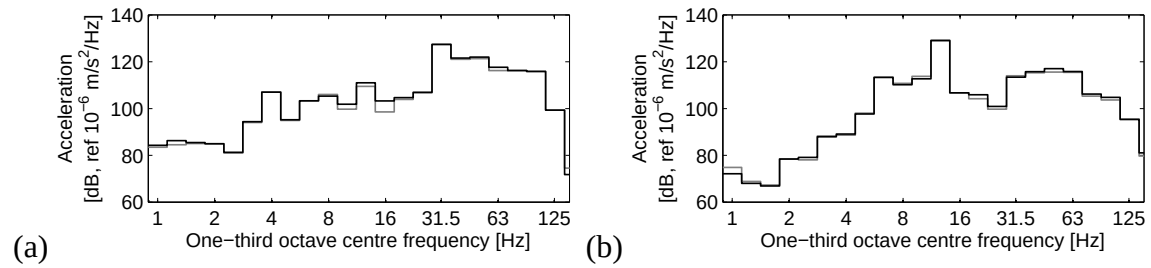

Figure 11: The computed total response (black line) and the computed quasi-static (grey line) one-third octave band spectra of the vertical acceleration at the center of the mid-span deck for a HST travelling at (a) $v = 80$ m/s y (b) $V_{1,2} = 110$ m/s.

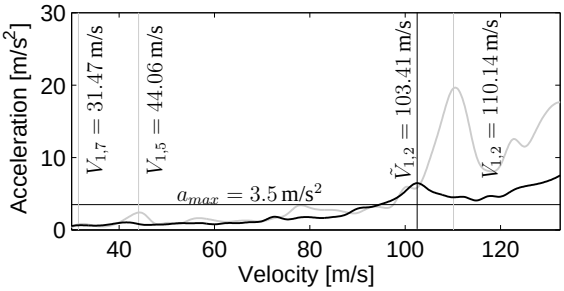

Figure 12: Maximum vertical acceleration at the mid-span center deck computed from SSI model (black line) and non-SSI model (grey line).

The resonant condition of a bridge excited by a row of moving forces can be expressed as follows [2, 5]:

$$V_{n,i} = \frac{f_n d}{i} \quad (n = 1, 2, ..., \, i = 1, 2, ...) \tag{19}$$

where, $V_{n,i}$ is the train speed, f_n is the n^{th} resonant frequency of the bridge and d is a characteristic distance of the moving loads.

Fig. 12 shows the maximum vertical acceleration at the center of mid-span deck in relation to the train speed passage. There is an increase of deck acceleration when the speed increases. Maximum levels are reached at resonant velocities of the first bending (symmetric) mode shape, considering the distance between bogies $d = 18.7$ m. Figure 12 shows the resonant velocities $V_{1,2} = 110.14$ m/s, $V_{1,5} = 44.06$ m/s and $V_{1,7} = 31.47$ m/s. The Spanish Standard [1] sets a limit state of vertical accelerations at $a_{max} = 3.5$ m/s^2, plotted in Fig. 12. The maximum acceleration at the center of the mid-span deck is below this limit in the range of operating speeds on current high speed lines. The response of the structure varies substantially when SSI is considered. Resonant velocities decrease due to variation of the dynamic behaviour of the structure. The maximum response occurs at $\tilde{V}_{1.2} = 103.41$ m/s. Moreover, it is observed that the maximum level of acceleration achieved in resonant regime is significantly lower when the soil-structure interaction is considered. The structural damping varies from $\zeta = 2$ % to $\tilde{\zeta} = 3.9$ %.

Fig. 13 shows the time histories and frequency content of the vertical acceleration at the center of mid-span deck for three train speed passage: $v = 80$ m/s, $\tilde{V}_{1,2} = 103.41$ m/s and $V_{1,2} = 110.14$ m/s. In the first case, the response obtained with both models corresponds with a non-resonant regime. The time history shows similar levels in both cases and the differences

are not significant. The response is governed by the bogie passing frequency, for the first bending (symmetric) mode and the first bending mode of the cross-section. The SSI produces an amplification of the response at the bogie passing frequency. In addition, the frequency response associated with the natural frequencies of the structure decreases. In resonant regime, the response of the structure shows a gradually increase of the vibrations with the successive bogie passage at the resonant velocities $\tilde{V}_{1,2}$ and $V_{1,2}$ (Fig. 13.(c),(e), respectively). The predominant frequency in the response are asociated with the first bending mode (Fig. 13.(d),(f)). The model without SSI does not estimate accurately the bridge response as can be seen in Fig. 13.(c),(d). Since the amplitude of the resonant vibration depend inversely on damping [2], the model without soil overestimates the response, as can be seen in Figs. 13.(e),(f).

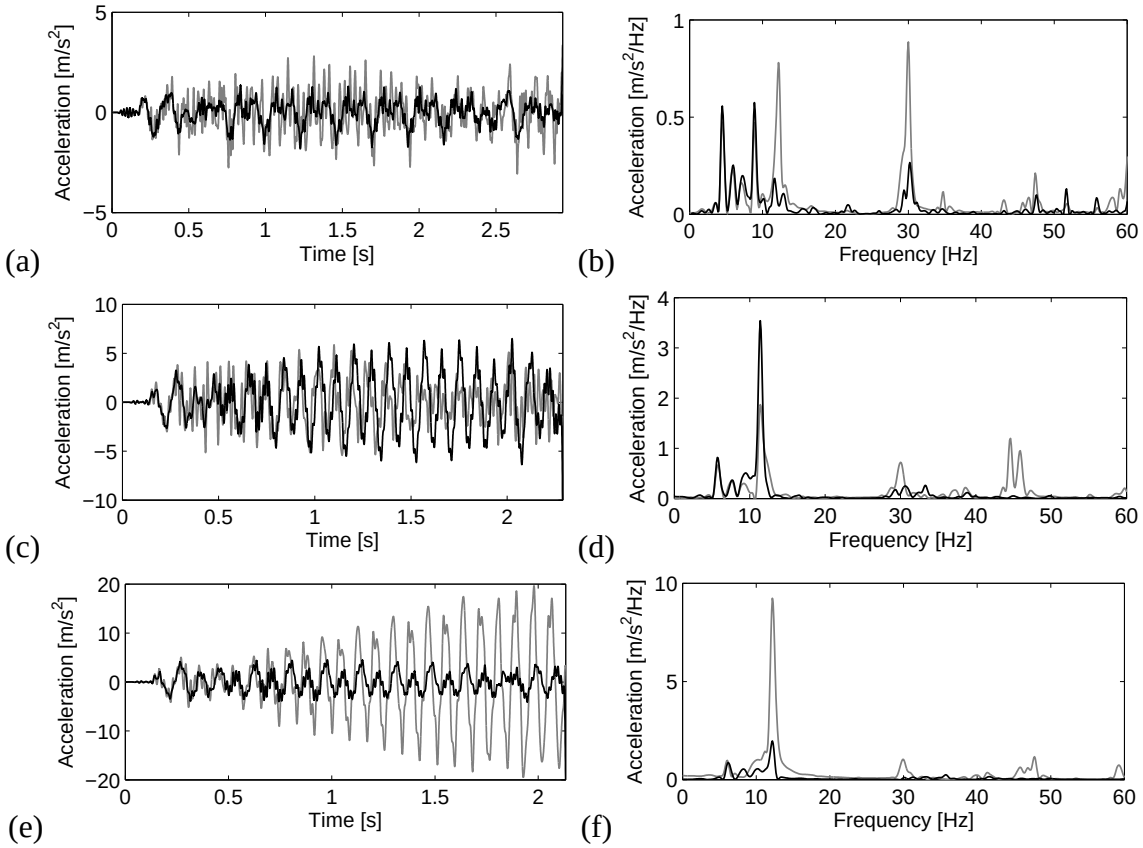

Figure 13: (a,c,e) Time histories and (b,d,f) frequency contents of the vertical acceleration at the mid-span center deck for a HST travelling at (a,b) $v = 80$ m/s, (c,d) $\tilde{V}_{1,2} = 103.41$ m/s y (e,f) $V_{1,2} = 110.14$ m/s, computed from the SSI model (black line) and the non-SSI model (grey line).

5 Conclusions

In this paper, a numerical model to predict vibrations on railway bridges has been presented. The numerical model is based on the three dimensional finite element and boundary element formulations in time domain. The articulated HST is modelled as a multi-body system. Therefore, the different excitation mechanisms can be considered accurately. The following conclusions can be drawn from the obtained results:

1. Transmitted force has a high frequency content that the moving force model does not

reproduce accurately due to vehicle's inertia effects are neglected.

2. Structure soil interaction produces a reduction in the natural frequencies and an increase of structural damping due to the additional flexibility level between the abutment and the soil.

3. Therefore, the resonant behaviour occurs at speeds lower than those predicted by the model without soil.

4. The amplitude of the resonant response regime depends on the structural damping ratio. So, it is necessary to take into account the influence of the SSI to estimate correctly the response.

Acknowledgments

This research is financed by the Ministerio de Ciencia e Innovación of Spain under the research project BIA2010-14843. The financial support is gratefully acknowledge. The support give by the Andalusian Scientific Computing Centre (CICA) is gratefull.

REFERENCES

[1] Ministerio de Fomento, *Instrucción sobre las acciones a considerar en el proyecto de puentes de ferrocarril IAPF07*, Ministerio de Fomento 2007

[2] L. Frýba, A rough assessment of railway bridges for high speed trains, *Engineering Structures* 23 (2001) 548-556.

[3] J. Li, M. Su, The resonant vibration for a simply supported girder bridge under high-speed trains, *Journal of Sound and Vibration* 224 (1999) 897-915

[4] S.H. Ju, H.T. Lin, Resonance characteristics of high-speed trains passing simply supported bridges, *Journal of Sound and Vibration* 267 (2003) 1127-1141

[5] H. Xia, N. Zhang, W.W. Guo, Analysis of resonance mechanism and conditions of train-bridge system, *Journal of Sound and Vibration* 297 (2006) 812-822.

[6] P. Museros, E. Alarcón, E, Influence of the second bending mode on the response of high-speed bridges at resonance, *Journal of Structural Engineering* 131 (2005) 405-415.

[7] P. Museros, M.D. Martinez-Rodrigo, Vibration control of simply supported beams under moving loads using fluid viscous dampers, *Journal of Sound and Vibration* 300 (2007) 292-315.

[8] M.D. Martínez-Rodrigo, J. Lavado, P. Museros, Transverse vibrations in existing railway bridges under resonant conditions: Single-track versus double-track configurations , *Engineering Structures* 32 (2010) 1861-1875.

[9] M.D. Martínez-Rodrigo, P. Museros, Optimal design of passive viscous dampers for controlling the resonant response of orthotropic plates under high-speed moving loads, *Journal of Sound and Vibration* (2010), doi:10.1016/j.jsv.2010.10.017

[10] A.V. Pesterev, L.A. Bergman, C.A. Tan, T.-C. Tsao, B. Yang, On the asymptotics of the solution of the moving oscillator problem, *Journal of Sound and Vibration* 260 (2003) 519-536.

[11] K. Liu, G. De Roeck, G. Lombaert, The effect of dynamic train-bridge interaction on the bridge response during a train passage, *Journal of Sound and Vibration* 325 (2009) 240-251.

[12] H. Takemiya, X.C. Bia, Shinkansen high-speed train induced ground vibratios in view of víaduct-ground interaction, *Soil Dynamics and Earthquake Engineering* 27 (2007) 506-520.

[13] H. Takemiya, Analyses of wave field from high-speed train on víaduct at shallow/deep soft grounds, *Journal of Sound and Vibration* 310 (2008) 631-649.

[14] M. Ülker-Kaustell, R. Karoumi, C. Pacoste, Simplified analysis of the dynamic soil-structure interaction of a portal frame railway bridge, *Engineering Structures* 32 (2010) 3692-3698.

[15] O.C. Zienkiewicz, *The Finite Element Method*, McGraw-Hill Company, London, 1977.

[16] J. Domínguez, *Boundary elements in dynamics*, Computational Mechanics Publications and Elsevier Applied Science, Southampton, 1993.

[17] P. Galvín, J. Domínguez, Analysis of ground motion due to moving surface loads induced by high-speed trains, *Engineering analysis with boundary elements* 30 (2007) 931–941.

[18] D.D. Barkan, *Dynamics of Bases and Foundations*, McGraw-Hill, New York, 1962.

[19] N.M. Newmark, A method of computation for structural dynamics, *ASCE Journal of the Engineering Mechanics Division* 85 (1959) 67–94.

[20] R.W Clough, J. Penzien *Dynamic of Structures*, McGraw-Hill, New York, 1975.

[21] P. Galvín, A. Romero, J. Domínguez, Fully three-dimensional analysis of high-speed train-track-soil-structure dynamic interaction , *Journal of Sound and Vibration* 329 (2010) 5147–5163.

[22] X. Sheng, C.J.C. Jones, D.J. Thompson, A theoretical model for ground vibration from trains generated by vertical track irregularities, *Journal of Sound and Vibration* 272 (2004) 937–965.

[23] C. Esveld, *Modern Railway Track*, MRT Productions,Zaltbommel, 2001.

[24] S.Y. Chang, Nonlinear error propagation analysis for explicit pseudodynamics algorithm, *Journal of engineering mechanics ASCE* 123 (2003) 841–850.

[25] G. Lombaert, G. Degrande, J. Kogut, S. François, The experimental validation of a numerical model for the prediction of railway induced vibrations, *Journal of Sound and Vibration* 297 (2006) 512–535.

[26] G. Lombaert, G. Degrande, Ground-borne vibration due to static and dynamic axle loads of InterCity and high-speed trains, *Journal of Sound and Vibration* 319 (2009) 1036–1066.

[27] International Organization for Standardization ISO 8608:1995, *Mechanical vibration road surface profiles-reporting of measured data*, 1995.